

Exact calculation of the energy contributions to the $T = 0$ random-field Ising model with metastable dynamics on the Bethe lattice

Xavier Illa,* Jordi Ortín,† and Eduard Vives‡

*Departament d'Estructura i Constituents de la Matèria, Facultat de Física, Universitat de Barcelona
Diagonal 647, 08028 Barcelona, Catalonia (Spain)*

(Dated: November 20, 2018)

We analyze the energy terms corresponding to the spin-spin exchange $\sum S_i S_j$ and spin-random field coupling $\sum S_i h_i$ of the zero temperature random-field Ising model on the Bethe lattice driven by an external field with metastable dynamics. Exact results are calculated as a function of the standard deviation of the disorder σ and the coordination number z , and compared with numerical simulations on random graphs for $z = 4$, for which a disorder-induced transition takes place.

PACS numbers: 75.60.Ej, 75.10.Nr, 05.50.+q, 75.40.Mg

I. INTRODUCTION

Hysteresis and metastability are intriguing phenomena with implications in both fundamental and applied physics [1]. They arise as a consequence of the existence of internal energy barriers that cannot be overcome by the system. A particularly interesting case is the so called “rate-independent” hysteresis, for which metastability is not a consequence of the fast driving rate but of the “athermal” character of the system. The energy barriers are so high compared with thermal fluctuations that effectively the system behaves at zero temperature, following a reproducible and deterministic metastable path when the external field is varied. Many experimental situations are known to be well approximated by this extreme case.

Several models have been useful for the characterization and description of rate independent hysteresis in different experimental systems. A very interesting microscopic model is the Random Field Ising model at $T = 0$ with metastable dynamics ($T = 0$ RFIM) [2]. It contains the three essential competing ingredients for the occurrence of “athermal” hysteresis: a ferromagnetic nearest-neighbour (n.n.) interaction term favouring long range order, a local energy term associated with quenched disorder, and a term describing the coupling of the magnetization to an external driving field. Although the model is formulated using a magnetic language it can be translated easily to other systems displaying athermal hysteresis.

During the last decade the $T = 0$ RFIM model has been used as a prototype for the understanding of many properties associated to hysteresis: return point memory, congruency, distribution of metastable states [3, 4], demagnetization process [5, 6], disorder induced critical points [7, 8, 9] and power-law distribution of the magnetization avalanches (Barkhausen noise) [10, 11]. Most of

these results are based on numerical simulations on finite lattices or on mean field analysis. Interestingly, however, non trivial analytical solutions can be obtained for the particular case of the $T = 0$ RFIM on Bethe lattices with coordination number z . The main hysteresis loop was solved seven years ago by Shukla, Dhar and Sethna [12, 13]. More recently partial loops [14, 15] and trajectories starting from states with “quenched” spins [16] have also been deduced. Here we present the explicit computation of the three energetic terms of the Hamiltonian \mathcal{H} for a generic values of σ and z [19]. Analytical results for all the contributions to \mathcal{H} give insight on the singular behaviour of the system at σ_c , and allows for a deeper understanding of the energy balances in the hysteresis loop.

The paper is organized as follows. In section II we summarize the details of the model. In section III we solve the different terms in the Hamiltonian. In section IV we present the results for the $z = 4$ case and compare with numerical simulations on random graphs. Finally, in section V, we study the energy dissipation.

II. MODEL

The RFIM is defined on a Bethe lattice with N sites and coordination number z . On each lattice site we define a spin variable S_i which takes values ± 1 . The Hamiltonian (magnetic enthalpy) reads:

$$\mathcal{H} = +U_e + U_d - HM \quad (1)$$

where H is the external driving field,

$$M(\{S_i\}) = \sum_{i=1}^N S_i \quad (2)$$

is the magnetization,

$$U_e(\{S_i\}) = -J \sum_{\langle i,j \rangle} S_i S_j \quad (3)$$

*Electronic address: xit@ecm.ub.es

†Electronic address: ortin@ecm.ub.es

‡Electronic address: eduard@ecm.ub.es

is the ferromagnetic exchange energy extending over all n.n. pairs, and

$$U_d(\{S_i\}) = - \sum_{i=1}^N h_i S_i \quad (4)$$

accounts for the energy interaction with quenched disorder. The random fields $\{h_i\}$ are independent and distributed according to a Gaussian probability density centered around zero:

$$f(h_i) = \frac{1}{\sqrt{2\pi\sigma}} e^{-\frac{h_i^2}{2\sigma^2}} \quad (5)$$

where σ is the standard deviation of the random fields and controls the amount of disorder in the system.

For the analysis of metastability and hysteresis loops we use a 1-spin-flip local relaxation dynamics. This is the standard choice used in previous studies of the metastable $T = 0$ RFIM [2]: each spin S_i flips individually according to the sign of its local field F_i given by:

$$F_i = J \sum_{j=1}^z S_j + H + h_i \quad (6)$$

where the first sum extends over the z neighbours of S_i . The complete lower branch of the hysteresis loop is obtained by adiabatically increasing H from $-\infty$ ($M = -N$) to $+\infty$ ($M = +N$).

In order to check the analytical results that will be presented we have also performed numerical simulations on random graphs with coordination number $z = 4$ and a range of sizes from $N = 10^4$ to $N = 10^6$. It is known that in the thermodynamic limit such numerical simulations agree with the analytical results for Bethe lattices [13]. For the simulations we start with a value of H negative enough so that the unique stable state is given by all the spins $S_i = -1$. We increase the external field H until F_i vanishes on a certain spin. The spin is then reversed keeping H constant. This reversal may destabilize some of the neighbouring spins, which are then reversed simultaneously (parallel updating). This is the beginning of an avalanche. The avalanches proceed until a new metastable situation with all the spins S_i aligned with their respective local fields F_i is reached. We can then continue increasing the external field H .

In the figures presented below numerical simulations correspond always to averages over several (~ 10) realizations of the random graph and many realizations of the random fields (~ 1000).

III. GENERAL SOLUTION FOR COORDINATION NUMBER z

Our goal is the computation of the different energetic terms in the Hamiltonian. The average over realizations

of the random fields of the three terms in the Hamiltonian gives:

$$\frac{\langle -HM \rangle}{N} = -H \langle S_i \rangle \equiv -Hm \quad (7)$$

$$\frac{\langle U_e \rangle}{N} = -\frac{1}{2} z J \langle S_i S_j \rangle \quad (8)$$

$$\frac{\langle U_d \rangle}{N} = -\langle h_i S_i \rangle \quad (9)$$

The averages on the right hand sides can be computed as follows:

$$\langle S_i \rangle = \sum_{\{S_i\}} S_i P(S_i) = P(+1) - P(-1) \quad (10)$$

where $P(S_i)$ is the probability for a spin to take a value ± 1 ,

$$\begin{aligned} \langle S_i S_j \rangle &= \sum_{\{S_i, S_j\}} S_i S_j P(S_i, S_j) = \\ &= P(+1, +1) + P(-1, -1) - 2P(+1, -1) \end{aligned} \quad (11)$$

where $P(S_i, S_j)$ is the probability for a nearest neighbour pair to be in the state (S_i, S_j) . This probability satisfies $P(+1, -1) = P(-1, +1)$. Finally

$$\begin{aligned} \langle h_i S_i \rangle &= \sum_{\{S_i\}} \int_{-\infty}^{+\infty} dh_i P(h_i, S_i) h_i S_i = \\ &= \int_{-\infty}^{+\infty} dh_i P(h_i, +1) h_i - \int_{-\infty}^{+\infty} dh_i P(h_i, -1) h_i \end{aligned} \quad (12)$$

where $P(h_i, S_i)$ is the probability for a site i of having a random field within $(h_i, h_i + dh_i)$ and a spin with state S_i .

At this point we follow Ref. 13. We define the probability $P(S_i|n)$ for a spin being in state S_i given a certain environment of nearest neighbours. This environment is fully characterized by the variable n ($0 \leq n \leq z$) which accounts for the number of neighbours in state +1 (see Fig. 1(a)). Clearly,

$$\begin{aligned} P(S_i = +1|n) &= \int_{-J(2n-z)-H}^{+\infty} dh_i f(h_i) = \\ &= \frac{1}{2} \operatorname{erfc} \left\{ \frac{-J(2n-z) - H}{\sqrt{2}\sigma} \right\} \end{aligned}$$

and

$$P(S_i = -1|n) = 1 - P(S_i = +1|n)$$

From Bayes formula one can write:

$$P(S_i) = \sum_{n=1}^z P(n) P(S_i|n) \quad (13)$$

where $P(n)$ is the probability for a site having an environment with n neighbouring spins in the state +1 (see Fig. 1(a)). According to Ref. 13,

$$P(n) = \binom{z}{n} P^{*n} (1 - P^*)^{(z-n)} \quad (14)$$

where P^* results from defining the conditional probability that a spin is +1 given that its parent spin (according to the hierarchy of the Bethe lattice) is down, and its descendent spins are relaxed. In a site deep enough inside a very big lattice (thermodynamic limit), this probability tends to be homogeneous and P^* is given by the self consistent equation [13]:

$$P^* = \sum_{n=0}^{z-1} P^{*n} (1 - P^*)^{z-1-n} P(S_i = +1|n) \quad (15)$$

Note that this equation implicitly contains the information on the fact that we are increasing the field monotonously from the negative fully saturated state.

By numerically obtaining P^* from (15) and using (14) and (13), the averaged magnetization in (10) can be obtained. This allows to calculate the averaged lower branch of the hysteresis loop.

In order to compute the terms (11) and (12) we apply Bayes formula again and write

$$P(S_i, S_j) = \sum_{l=1}^{z-1} \sum_{r=1}^{z-1} P(l, r) P(S_i, S_j | l, r) \quad (16)$$

$$P(h_i, S_i) = \sum_{n=1}^z P(n) P(h_i, S_i | n), \quad (17)$$

where $P(S_i, S_j | l, r)$ and $P(h_i, S_i | n)$ are conditional probabilities given a certain environment and $P(l, r)$ is the probability for a pair having an environment with l spins in the state +1 in the left neighbourhood and r spins in the state +1 in the right neighbourhood (see Fig. 1(b)). This is the generalitation of $P(n)$ for the description of the environment of a pair of spins.

A. Calculation of $P(S_i, S_j)$

The calculation of $P(S_i, S_j)$ starts by generalizing Eq. (14) to

$$\begin{aligned} P(l, r) &= g(l, r) P^{*l} (1 - P^*)^{(z-1-l)} P^{*r} (1 - P^*)^{(z-1-r)} = \\ &= g(l, r) P^{*l+r} (1 - P^*)^{(2z-2-r-l)} \end{aligned} \quad (18)$$

where

$$g(l, r) = \binom{z-1}{l} \binom{z-1}{r} \quad (19)$$

The conditional probabilities for a pair of spins given a certain environment, $P(S_i, S_j | l, r)$, can be written as

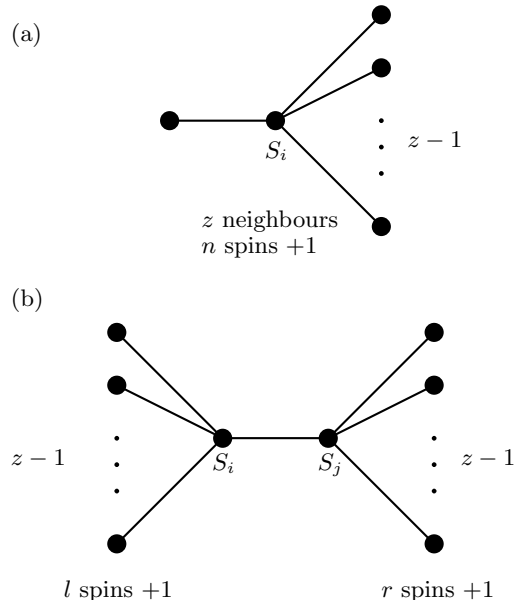


FIG. 1: Schematic representation of the environment of (a) a single site and (b) a pair. The variables n, l, r account for the number of spins +1.

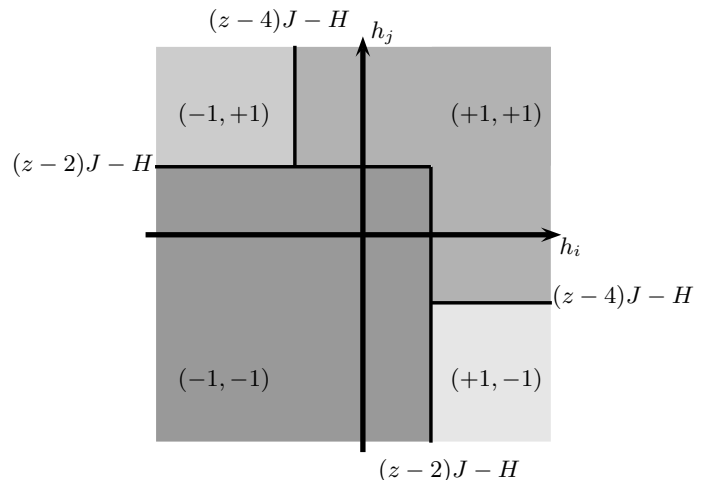


FIG. 2: The (h_i, h_j) plane divided in different areas (different color) corresponding to the final state of spins (S_i, S_j) for a fixed environment $l = 1, r = 1$. These areas correspond to the domains D of integration in Eq. (20).

double integrals of the random field distribution on a certain domain in the $h_i - h_j$ plane, i.e.

$$P(S_i, S_j | l, r) = \int \int_D f(h_i) f(h_j) dh_i dh_j \quad (20)$$

Figure 2 shows an example of such domains corresponding to the environment $l = 1$ and $r = 1$. The plots corresponding to other environments are obtained by translation of this case. Therefore:

$$P(-1, -1|l, r) = [1 - P(S_i = +1|l)] [1 - P(S_i = +1|r)] \quad (21)$$

$$P(+1, -1|l, r) = P(S_i = +1|l) [1 - P(S_i = +1|r + 1)] \quad (22)$$

$$P(-1, +1|l, r) = [1 - P(S_i = +1|l + 1)] P(S_i = +1|r) \quad (23)$$

$$P(+1, +1|l, r) = P(S_i = +1|l + 1)P(S_i = +1|r) + P(S_i = +1|l) [P(S_i = +1|r + 1) - P(S_i = +1|r)] \quad (24)$$

From these equations and using (18) and (16) one can obtain the correlation $\langle S_i S_j \rangle$ needed for the computation of Eq. (11).

B. Calculation of $P(h_i, S_i)$

The computation of $P(h_i, S_i)$ is straightforward noting that $P(h_i, S_i|n)$ can be computed as tails of the gaussian distribution $f(h_i)$ as:

$$P(h_i, +1|n) = \begin{cases} 0 & h_i < (z - 2n)J - H \\ f(h_i) & h_i > (z - 2n)J - H \end{cases} \quad (25)$$

$$P(h_i, -1|n) = \begin{cases} f(h_i) & h_i < (z - 2n)J - H \\ 0 & h_i > (z - 2n)J - H \end{cases} \quad (26)$$

Thus, using (14) and (17) one can compute $\langle h_i S_i \rangle$ needed for the computation of Eq. (12).

IV. NUMERICAL SOLUTION FOR THE CASE $z = 4$

The case with coordination number $z = 4$ is interesting because it is known [13] to display a disorder induced phase transition between smooth hysteresis loops for $\sigma > \sigma_c = 1.78125$ and discontinuous hysteresis loops for $\sigma < \sigma_c$. We present the results obtained by numerically solving the equation of the previous section for $z = 4$. In particular the real roots of Eq. (15) are found with a bisection method restricted to the interval $0 \leq P^* \leq 1$.

Figure 3 shows the m - H diagram corresponding to four different amounts of disorder σ . Note that the data represented corresponds only to the lower branch of the hysteresis loop for increasing the external field H .

The discontinuity in the $m(H)$ branch, as was pointed out in Ref. [13], arises from the fact that the solution of equation (15) is trivalued for $\sigma < \sigma_c$ in a certain field range $H_1 < H < H_2$. The three roots of Eq. (15) generate the s-shape curve in the $m - H$ diagram than can be

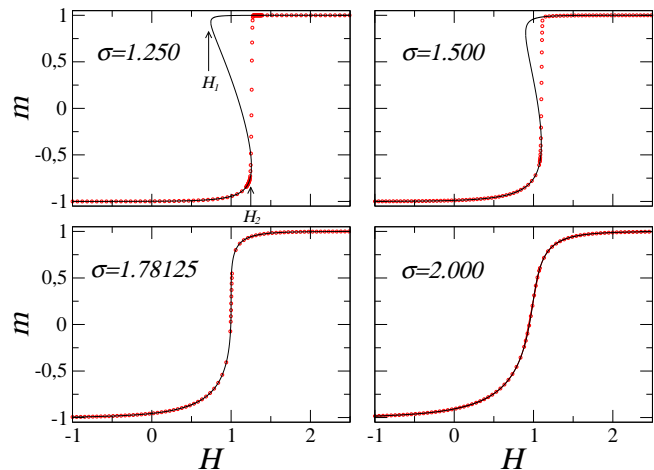


FIG. 3: Lower branches of the hysteresis loop corresponding to $z = 4$ and different amounts of disorder. Exact results (continuous lines) are compared with numerical simulations (dotted lines). Simulations correspond to a random graph with $N = 10^5$ and averages over 1000 different realizations of disorder

observed in Fig. 3 for $\sigma < \sigma_c$. Nevertheless, numerical simulations show that only one of the roots has physical meaning. In the case of increasing field, only the lower m branch is obtained in the simulations, and the discontinuity occurs at H_2 where this lower branch of the s-shape curve joins the intermediate branch and disappears. To our knowledge there is no clear physical explanation for this fact and, a priori, the jump could occur at any field in the range H_1 - H_2 . A stability criterium would be desirable. In this respect we note that in a very recent paper [4], it has been speculated that the s-shape curve is related to the boundary of the density of 1-spin-flip metastable states [17]. It is also important to notice that the result of numerical simulations depends on system size, as shown in Fig. 4. Only in the thermodynamic limit ($N \rightarrow \infty$) the data from numerical simulations would follow exactly the lower branch of the theoretical curve up to H_2 .

Figure 5 shows the behaviour of U_e corresponding to the same four cases as in Fig. 3. Below σ_c the three roots of Eq. (15) generate a lace function. Numerical simulations follow continuously one of the roots until H_2 where they jump to the lower exchange energy branch. Note that there is an intermediate field H_3 (crossing point of the lace) where two of the roots correspond to the same value of U_e .

Figure 6 shows the behaviour of U_d [20]. A similar lace shape is obtained. We note, that the crossing points H'_3 (for $\sigma < \sigma_c$) are different from H_3 in the U_e curve. As σ tends to σ_c the fields H_1 , H_2 , H_3 , and H'_3 all tend to the critical value $H_c = 1$ [13].

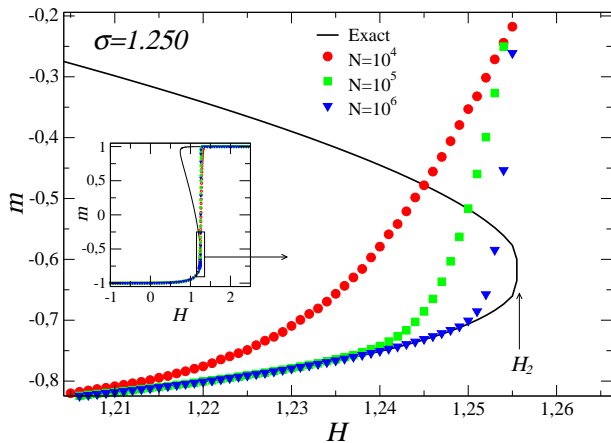


FIG. 4: Examples of finite size dependence of the lower branch of the hysteresis loop. Symbols correspond to simulations on random graphs with increasing sizes as indicated by the legend. The continuous line corresponds to the exact solution.

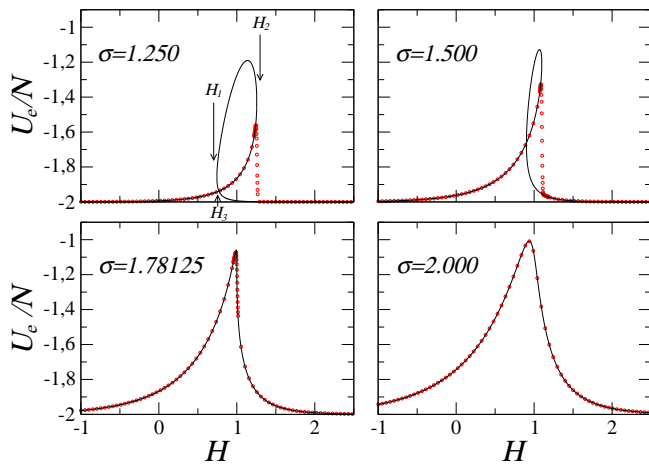


FIG. 5: Exchange energy behaviour corresponding to the same cases as in Fig. 3. Lines correspond to numerical solution of the exact equations and dots correspond to numerical simulation on random graphs.

In Fig. 7 we show the behaviour of the total Hamiltonian (magnetic enthalpy) \mathcal{H} , corresponding to the same four cases as before. The plots show that, in the trivalued region, the numerical simulations choose the branch with maximum \mathcal{H} , which is clearly a non-equilibrium path.

V. ENERGY DISSIPATION

The fact of having obtained separately m , U_e , and U_d , as functions of H , allows an exact computation of the energy dissipated by the system Q . It can be calculated

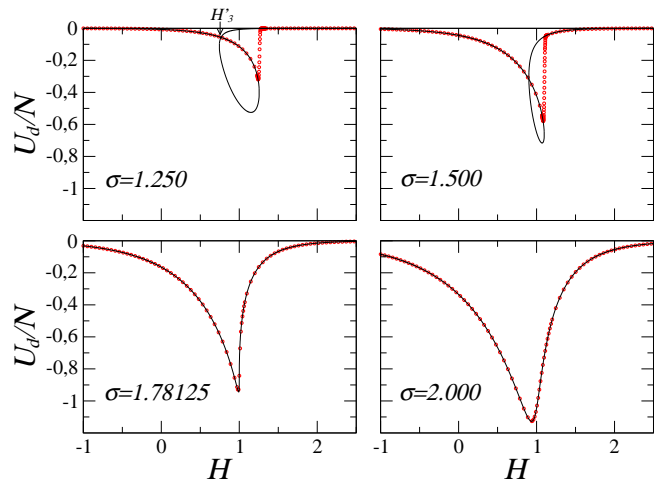


FIG. 6: Disorder-coupling energy corresponding to the same cases as in Fig. 3. Lines correspond to numerical solution of the exact equations and dots correspond to numerical simulation on random graphs.

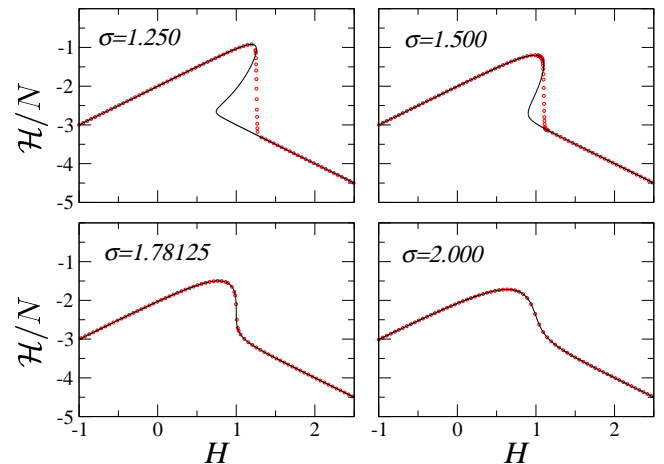


FIG. 7: Behaviour of the Hamiltonian \mathcal{H} as a function of the external field H corresponding to the same four cases as the previous figures. Numerical solution of the exact equations are shown with a continuous line, whereas numerical simulations of random graphs are shown with a dotted line.

by integration along the non-equilibrium path [18]:

$$Q = \Delta U - \int H dM, \quad (27)$$

where $\Delta U = \Delta U_e + \Delta U_d$ (internal energy difference between the initial and final states). Starting from $H = -\infty$, the path integral over the trajectory computed in the previous section can be written in the form:

$$\frac{Q(-\infty \rightarrow H')}{N} = \frac{U(H')}{N} + \frac{1}{2}zJ - \int_{-\infty}^{H'} H dm. \quad (28)$$

Figure 8 shows the result obtained from this expression for $z = 4$ and different values of σ . For those cases for

which $\sigma < \sigma_c$ the energy dissipated has been computed for three different trajectories (indicated by dashed or continuous lines), all of them compatible with the theoretical (numerical) solution of $m(H)$, $U_e(H)$, and $U_d(H)$: the first one assumes that the transition to the upper branch of $m(H)$ takes place at $H = H_1$, the second one at an intermediate value of the field $H = (H_1 + H_2)/2$, and the third one at $H = H_2$. Of these trajectories, we verify that the one jumping at H_2 (the trajectory chosen by the system in the numerical simulations) is the one of maximum energy dissipation (Q most negative).

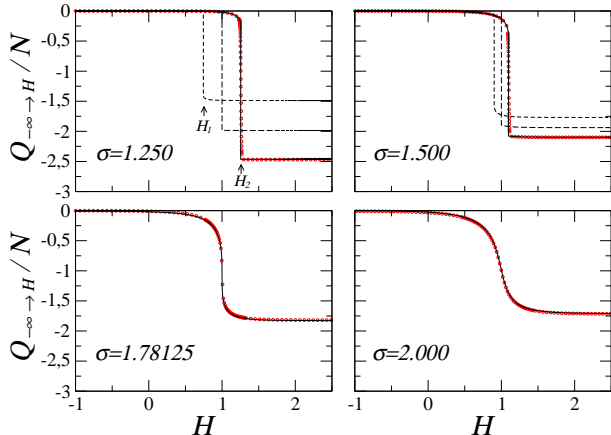


FIG. 8: Energy dissipated along the metastable path $-\infty \rightarrow H$, computed from Eq. (28). For $\sigma < \sigma_c$ we compare three possible trajectories which differ in the field at which the transition occurs (see text for details). The dotted line is the result of our numerical simulations on random graphs.

In Fig. 9 we compare the energy dissipation associated with the magnetization transition jump at H_2 ($Q_T = \Delta\mathcal{H}$) with the total energy dissipated along the full path $Q_{-\infty \rightarrow \infty}$. One can see that for $\sigma < \sigma_c$ the dissipation at the transition Q_T represents a large fraction of the total dissipation.

VI. SUMMARY AND CONCLUSIONS

We have studied the RFIM on a Bethe lattice with a 1-spin-flip local relaxation metastable dynamics, following the method proposed in Refs. 13, 15. We have extended

the calculations and computed the different energy terms in the Hamiltonian which account for the spin-spin exchange energy (U_e), the spin-random field coupling term (U_d), and the energy associated with the external driving field ($-HM$). The analysis of the Bethe lattice with coordination numbers $z > 3$ allows to understand (with analytic equations) the role played by each energy term in the disorder induced phase transition that separates the phase with smooth hysteresis loop from the phase with discontinuous hysteresis loop. The availability of the separate energy terms allows the study of the energy dissipation as a function of the external field along the hysteresis loop.

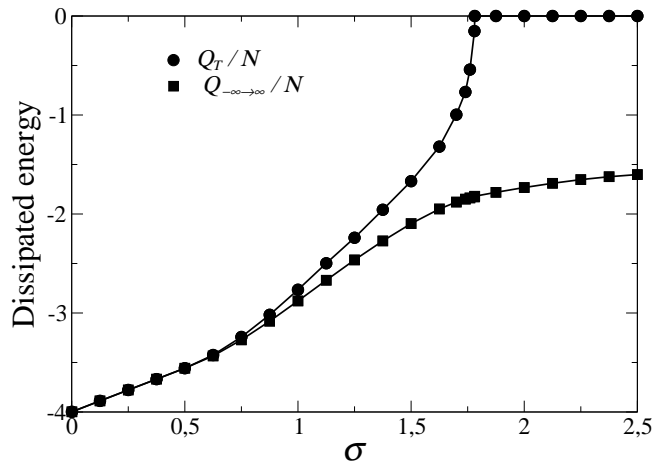


FIG. 9: Comparison of the energy dissipated at the transition jump Q_T (\bullet) with the total energy dissipated along the full path $Q_{-\infty \rightarrow \infty}$ (\blacksquare).

VII. ACKNOWLEDGEMENTS

We acknowledge fruitful comments from Prabodh Shukla. This research has received financial support through projects MAT2004-01291 (CICyT, Spain), BQU2003-05042-C02-02, BFM2003-07749-C05-04 (MEC, Spain), SGR-2000-00433, SGR-2001-00066 (DURSI, Generalitat de Catalunya). We acknowledge a supercomputing project from CESCA (Catalunya). X.Illa acknowledges financial support from DGI-MEC.

[1] G.Bertotti, *Hysteresis in magnetism*, Electromagnetism series (Academic Press, Sand Diego, 1998).
 [2] J. P. Sethna, K. Dahmen, S. Kartha, J. A. Krumhansl, B. W. Roberts, and J. D. Shore, Phys. Rev. Lett. **70**, 3347 (1993).
 [3] V.Basso and A.Magni, Physica B **343**, 275 (2004).

[4] F.Detcheverry, M.L.Rosinberg, and G.Tarjus, cond-mat/0411677 (2004).
 [5] L. Dante, G. Durin, A. Magni, and S. Zapperi, Phys. Rev. B **65**, 144441 (2002).
 [6] F.Colaiori, A.Gabrielli, and S.Zapperi, Phys. Rev. B **65**, 224404 (2004).

- [7] K. A. Dahmen and J.P.Sethna, Phys. Rev. Lett. **71**, 3222 (1993).
- [8] K. A. Dahmen and J.P.Sethna, Phys. Rev. B **53**, 14872 (1996).
- [9] O. Perković, K. A. Dahmen, and J.P.Sethna, Phys. Rev. B **59**, 6106 (1999).
- [10] F.J.Pérez-Reche and E.Vives, Phys. Rev. B **67**, 134421 (2003).
- [11] F.J.Pérez-Reche and E.Vives, Phys. Rev. B **70**, to be published (2004).
- [12] P. Shukla, Physica A **233**, 235 (1996).
- [13] D. Dhar, P. Shukla, and J. Sethna, J. Phys. A: Math. Gen. **233**, 235 (1997).
- [14] P. Shukla, Phys. Rev. E **62**, 4725 (2000).
- [15] P. Shukla, Phys. Rev. E **63**, 027102 (2001).
- [16] P.Shukla and R.Kharwanlang, cond-mat/0406749 (2004).
- [17] E.Vives, M.L.Rosinberg, and G.Tarjus, cond-mat/0411330 (2004).
- [18] J. Ortín and J. Goicoechea, Phys. Rev. B **58**, 5628 (1998).
- [19] During the final stages of this work, we were aware of an unpublished document by L.Dante that contains basically the same calculation restricted to the case $z = 2$.
- [20] We note that this energy term, can be explicitly written as an analytical function of P^* , but we have omitted it for simplicity.